NUCLEAR REACTIONS -- THEORY

PRE-EQUILIBRIUM PARTICLE EMISSION AND CRITICAL EXPONENT ANALYSIS

Wolfgang Bauer and Alexander Botvina[a]

The premier goal of medium and high energy heavy-ion reactions is the exploration of the nuclear phase diagram. On theoretical grounds we expect infinite nuclear matter to undergo at least two distinct phase transitions. One is the deconfinement or quark-gluon-plasma phase transition. The other is a "liquid-gas" type phase transition. It is believed to be of first order, terminating at the critical point in a second order transition. In nuclear multifragmentation reactions one attempts to map out the liquid-gas coexistence region and locate the critical point. Recently the EOS TPC collaboration used the reaction 1 A GeV Au + C in an attempt to reach the critical point of nuclear matter and determine the critical exponents in the spectator fragmentation of the residue of the gold nucleus[1,2]

In the present study, we have constructed a hybrid model, in which the pre-equilibrium energy deposition and resulting residue size are calculated in the framework of an intra-nuclear cascade (INC) model[4] and in which we calculate the decay of the residue within a percolation model[3] or statistical multifragmentation model (SMM)[5] framework.[6]

One can see that the INC/percolation model shows an amazing degree of agreement with the data. From this we come to two conclusions:

- We agree with the main statement of the Ref. 1: The data in Fig. 1 are consistent with a scenario in which some of the fragmentation events occurred close to the critical point of a second order fragmentation phase transition.
- We disagree with Ref. 1 on the exact numerical values of the critical exponents of the transition. We find that the values extracted in Ref. 1 can be explained on the basis of finite-size effect and distortions introduced by the analysis method. From the agreement between the INC/percolation model and the data, one may instead conclude that the critical exponents of the nuclear fragmentation phase transition are reasonably close to the ones of a percolation transition.

a. On leave from Institute for Nuclear Research, 117312 Moscow, Russia. Present address: Hahn-Meitner-Institut, 14109 Berlin, Germany.

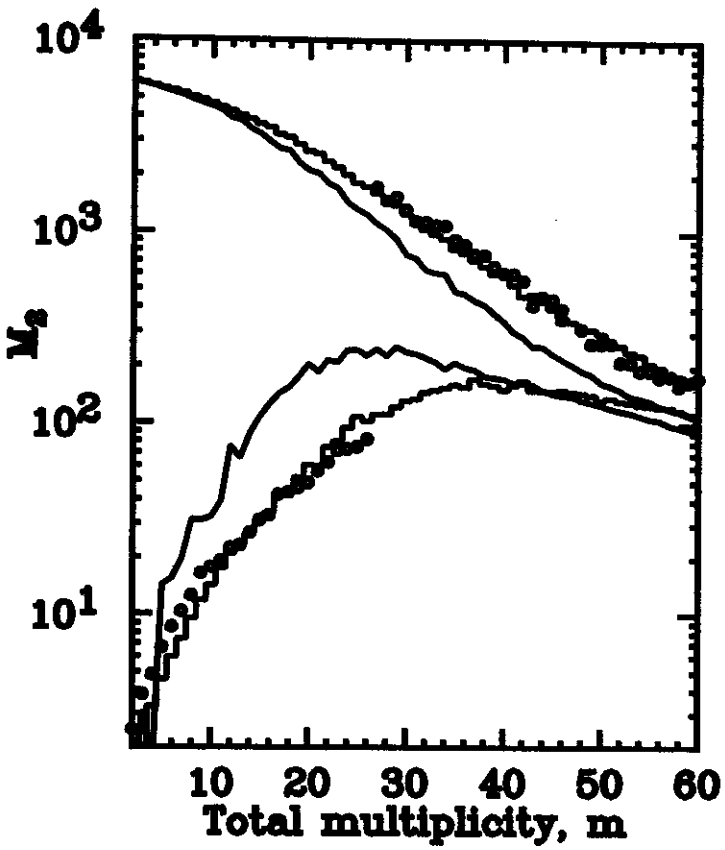

Figure 1: Second moment of the charge distribution as a function of the charged particle multiplicity for the reaction 1 A GeV Au + C. Histogram: INC/percolation, line: INC/SMM, circles: data[2].

References

1. M.L. Gilkes et al., Phys. Rev. Lett. 73, 1590 (1994).
2. H.G. Ritter et al., Nucl. Phys. A 583, 491c (1995).
3. W. Bauer, D.R. Dean, U. Mosel, and U. Post, Phys. Lett. 150B, 53 (1985); W. Bauer, Phys. Rev. C 38, 1927 (1988).
4. A.S. Botvina et al., Yad. Fiz. (Sov. J. Nucl. Phys.) 57, 667 (1994).
5. A.S. Botvina et al., Nucl. Phys. A 507, 649 (1990).
6. W. Bauer and A. Botvina, Phys. Rev. C 52, R1760 (1995).

RADIAL FLOW IN AU+AU COLLISIONS FROM 0.2 TO 2 GEV/A

F. Daffin, K. Haglin, W. Bauer

The expansion of hot, excited nuclear matter formed in collisions of heavy ions is governed by the fundamental forces of nature. In an effort to understand their effects, we have turned to studies of these collisions through observables sensitive to the dynamics they govern. Such observables as collective flow phenomena[1]-[8] have been used in the past with success. Flow originates when nuclear matter from nucleus-nucleus collisions attains a strongly correlated momentum distribution principally through effective strong interactions.

Of the models used to simulate heavy ion collisions at intermediate energies, the BUU model[9]-[15] is among the most fruitful. However, our BUU code evolves the single particle phase-space distribution and there is no self-consistent provision in the nuclear mean field for higher order correlations. The result is a numerical model that is successful at predicting and providing insight into single particle observables[2,4,5], but at the same time not suited to providing the same for clustering and fragmentation.

The success of BUU in predicting and reproducing the empirical transverse, in-plane proton momentum distributions[4,5], one may wonder whether radial flow can be used to discriminate between model parameters. Our goal was to compare calculations of low rapidity yields of protons and light fragments from central Au+Au collisions to recent results from the EOS-TPC[8]. Spectra were analyzed using a radially expanding thermal model[16] from which radial flow velocities and temperatures were extracted.

We use a coalescence model to convert the single particle phase-space distribution evolved in BUU to freeze-out into a final-state distribution of free protons, deuterons, tritons, ^{3}He and alpha particles. Then using χ^2/ν minimization, we fit the resulting spectra to thermal yet radially expanding distributions to assign a common temperature and expansion velocity for the collision volume.

The BUU formalism was used to simulate Au+Au collisions at energies 0.25, 0.60, 1.0, 1.5 and 2.0 GeV/A with impact-parameter-averaging, $b \leq 3$ fm, and a stiff (compressibility K=380 MeV) momentum-dependent nuclear mean field. The nucleons scattered with the free-space cross sections ($\alpha = 0$). The system was evolved until the collision rate dropped to less than one collision per ensemble per time step. At this point reaction dynamics responsible for clustering becomes important. We matched the experimental acceptance of $\theta_{cm} = 90° \pm 15°$ relative to the beam axis.

In addition to proton spectra, light fragments were measured. Since our BUU has no self-consistent provision for the production of light fragments, a coalescence algorithm was needed to convert the phase-space distribution of protons and neutrons at freeze-out into singles plus composites. Deuterons were formed whenever a proton and a neutron were within a critical radius in configuration space and the same proton and neutron were within a critical radius in momentum space. These critical radii were fixed by minimizing the difference between the final-state proton spectra from the BUU calculation and that from experiment. We found $\Delta R_{deuteron} = 1.5\,\mathrm{fm}$ and $\Delta P_{deuteron} = 100\,\mathrm{MeV/c}$. Critical radii for heavier fragments were simply increased according to $R_i \propto A_i^{1/3}$, where i is the fragment species.

Spectra of protons, deuterons, tritons, ^{3}He and alphas were analyzed using a radially expanding thermal model[16]. Here the fragments are assumed to possess a thermal velocity distribution characterized by a temperature in Maxwell-Boltzmann statistics, and an overall radial velocity. In the global rest

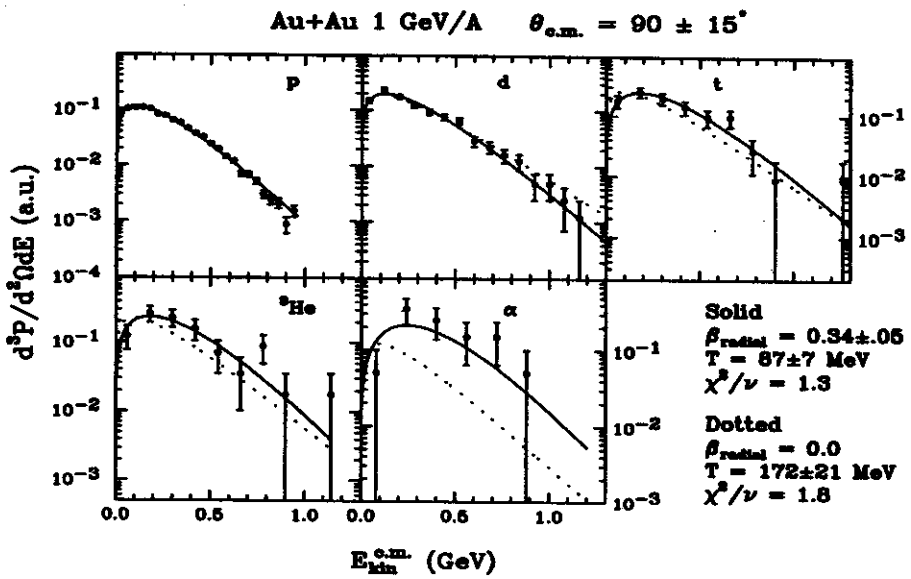

Fig. 1: Spectra of BUU + Coalescence. Global temperature and radial flow velocity were obtained by fitting the radially expanding thermal model[16] to deuterons, tritons, ^{3}He, and alphas. Dotted lines are the global fits for a radial flow velocity of zero.

frame the resultant distribution is

$$\frac{d^3N}{dp^3} \sim \exp\left(-\gamma E/T\right)\left[\left(\frac{\gamma+T}{E}\right)\frac{\sinh(\alpha)}{\alpha} - \frac{T}{E}\cosh(\alpha)\right], \tag{1}$$

where $\gamma \equiv 1/\sqrt{1-\beta^2}$, $\alpha \equiv \gamma\beta p/T$, T is temperature and $\beta \equiv v/c$ is the radial flow velocity. The spectra were fit to Eq.(1) by fixing the overall normalization and varying T and β to obtain a minimum χ^2/ν. Global fits constituted simultaneous fits to deuterons, ^{3}He, tritons, and alphas since the proton spectrum was used to fix the critical radii for coalescence.

Our results at 1 GeV/A appear in Figure 1. The temperature and radial flow velocity are consistent with those obtained in experiment[8] within uncertainties, and provides good evidence that BUU+coalescence is capable of reproducing this combination of radial and thermal motion in light fragments. Our simultaneous fit to the fragment spectra with a nonzero radial flow velocity gave a minimum χ^2/ν of 1.3. Forcing a zero radial flow velocity yields a minimum χ^2/ν of 1.8, in keeping with, though not as dramatic as, the results of the EOS-TPC study[8]. Without absolute cross sections, normalizations were free parameters in our minimization of χ^2/ν.

We extended our impact-parameter-averaged investigation to energies 0.25, 0.60, 1.5, and 2 GeV/A. The results are presented in Figure 2. Here one can see that results from the calculations have significant overlap with experiment. Temperatures extracted from BUU+Coalescence simulations agree well with those extracted from experiment, whereas our results for radial flow velocity agree less well. They do suggest a saturation of radial flow velocity as beam energy is increased beyond 1GeV/A. This is consistent with AGS data[17].

The microscopic features of the BUU transport code seem to have little influence on the radial flow velocity. The numerical models used in the EOS-TPC study[8] also showed the radial flow velocity to have

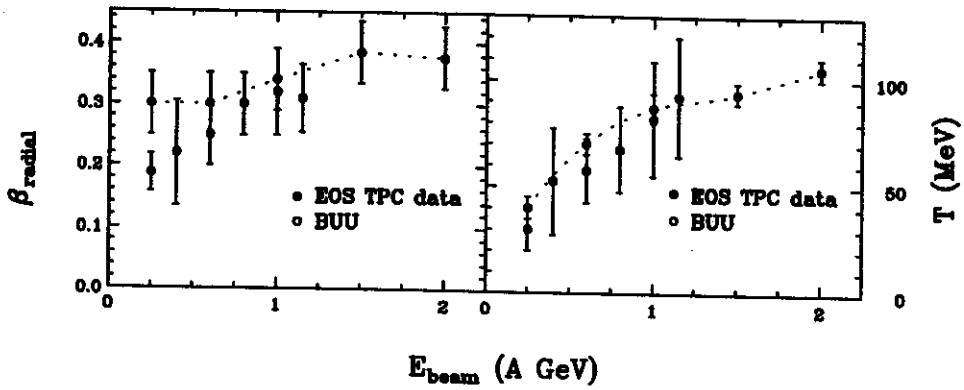

Fig. 2: Excitation function of the radial flow velocity β and temperature.

little dependence on the equation of state (EOS) used. Indeed, we cannot discern any EOS dependence at this time within our estimated uncertainties. Radial flow will not develop within $\theta_{cm} = 90° \pm 15°$ of the beam axis without nucleon-nucleon collisions. In simulations at $b = 2$ fm, E_{beam}=1 GeV/A, that were allowed to reach maximum compression before σ_{nn} was set to zero, almost no matter obtained rapidities low enough to meet the kinematic selection angle. However, we did see evidence that directed flow could be observed in those simulations. Thus we conclude that both nuclear mean fields and nucleon-nucleon collisions are important in the development of radial flow, and that it is likely that they offer roughly equal contributions to radial flow. We find that the magnitude of the radial flow, as opposed to the total radial kinetic energy, is chiefly governed by the beam energy.

There is, however, some sensitivity in the temperature of the light fragment spectra to momentum dependence in the nuclear mean field, as well as to the influence of the Coulomb field (see Table 1).

References

1. P. Danielewicz and G. Odyniec, Phys. Lett. 157B, 146, (1985).
2. G. F. Bertsch, W. G. Lynch and M. B. Tsang, Phys. Lett. 189B, 384, (1987).
3. C. A. Ogilvie, D. A. Cebra, J. Clayton, P. Danielewicz, S. Howden, J. Karn, A. Nadasen, A. Vander Molen, G. D. Westfall, W. K. Wilson, and J. S. Winfield, Phys. Rev. C 40, 2592, (1989).
4. C. Gale, G. M. Welke, M. Prakash, S. J. Lee, and S. Das Gupta, Phys. Rev. C 41, 1545 (1990).
5. G. D. Westfall, C. A. Ogilvie, D. A. Cebra, W. K. Wilson, A. Vander Molen, W. Bauer, J. S. Winfield, D. Krofcheck, J. Karn, S. Howden, T. Li, R. Lacey, K. Tyson and M. Cronqvist, Nucl. Phys. A519, 141, (1990).
6. C. A. Ogilvie, W. Bauer, D. A. Cebra, J. Clayton, S. Howden, J. Karn, A. Nadasen, A. Vander Molen, G. D. Westfall, W. K. Wilson and J. S. Winfield, Phys. Rev. C 42, R10, (1990).
7. G. D. Westfall, W. Bauer, D. Craig, M. Cronqvist, E. Gualtieri, S. Hannuschke, S. Klakow, T. Li, T. Reposeur, A. M. Vander Molen, W. K. Wilson, J. S. Winfield, J. Yee, S. J. Yenellow, R. Lacey, A. Elmaani, J. Lauret, A. Nadasen and E. Norbeck, Phys. Rev. Lett. 71, 1986, (1993).
8. M. A. Lisa, *et. al.*, Phys. Rev. Lett. 75, 2662, (1995).
9. G. F. Bertsch, H. Kruse and S. Das Gupta, Phys. Rev. C 29, 673, (1984).
10. J. Aichelin and G. F. Bertsch, Phys. Rev. C 31, 1730, (1985).
11. H. Stöcker and W. Greiner, Phys. Rep. 137, 277, (1986).
12. G. F. Bertsch and S. Das Gupta, Phys. Rep. 160, 189 (1988).
13. V. de la Mota, F. Sebille, M. Farine, B. Remaud, and P. Schuck, Phys. Rev. C 46, 677, (1991).
14. W. Bauer, J. P. Bondorf, R. Donangelo, R. Elmér, B. Jakobsson, H. Schulz, F. Schussler, and K. Sneppen, Phys. Rev. C 47, R1838, (1993).
15. W. K. Wilson, W. Bauer, C. Cebra, M. Cronqvist, D. Krofchek, R. Lacey, T. Li, A. Nadasen, E. Norbeck, T. Reposeur, A. Vander Molen, C. A. Ogilvie, G. D. Westfall, J. S. Winfeld, and J. Yee, Phys. Rev. C 51, 3136, (1995).

EOS	T±5 (MeV)	$\beta \pm 0.05$
Coulomb, $\alpha = 0$		
Stiff	70	0.35
Soft	80	0.35
Soft $\vec{p}$	75	0.35
Stiff $\vec{p}$	90	0.35
No Coulomb, $\alpha = 0$		
Stiff	70	0.35
Soft	70	0.30
Soft $\vec{p}$	95	0.35
Stiff $\vec{p}$	95	0.35
Coulomb, $\alpha = -0.20$		
Stiff	75	0.35
Soft	65	0.35
Soft $\vec{p}$	80	0.35
Stiff $\vec{p}$	75	0.40
Coulomb, $\alpha = -0.50$		
Stiff	70	0.35
Soft	65	0.35
Soft $\vec{p}$	70	0.35
Stiff $\vec{p}$	90	0.35

Table 1: Effects of the microscopic features of BUU on apparent temperature and radial flow velocity.

16. P. J. Siemens, J. O. Rasmussen, Phys. Rev. Lett. 42, 880 (1979).
17. J. Harris, W. Lynch, B. Zajc, W. Bauer, M. Gyulassy, J. Natowitz, J. Stachel, Report of the Intermediate and High Energy Heavy-Ion Reactions: NSAC/DNP Town Meeting-Brookhaven National Laboratory, January 27-28, 1995.

NUCLEAR FLOW RESULTING FROM CONSISTENT BOLTZMANN ALGORITHMS

Gerd Kortemeyer, Frank Daffin, and Wolfgang Bauer

1. INTRODUCTION

Within the semi-classical particle-based Boltzmann-Uehling-Uhlenbeck (BUU) approach for the simulation of Relativistic Heavy Ion Collisions, the collision term can be represented in different ways. One particular implementation is the Direct Simulation Monte Carlo approach (DSMC), see for example Lang et al. [1], and Danielewicz [6]. In this approach, collisions between the testparticles are not generated through geometrical and particle-trajectory based criteria, but stochastically in a way that the correct collision rate is reproduced. In a collision only momenta and energy of the particles are changed, while the particles themselves stay in place until the next advection step – the particles are assumed to be pointlike.

It was suggested that in order to reproduce a Hard-Sphere Boltzmann Equation, the DSMC approach should be extended by an additional advection that should take place after any collision [2], and by a modification the collision probability itself [2,3] (Enskog Theory).

This advection is supposed to push the collision partners away from each other according to their hard-sphere radius, and the collision probability is adjusted to take into account the excluded volume of the hard spheres and screening and shadowing effects. The modified DSMC method is called Consistent Boltzmann Algorithm (CBA). The modifications ensure a non-vanishing second virial and change the equation of state for the scattering process from that of an ideal gas to that of a hard-sphere gas; we analyse their effect on the calculated value of directed nuclear collective flow in heavy ion collisions, and find that the flow slightly increases.

2. RESULTS

Our numerical calculation is based on the MSU BUU-code by Bauer et al. which was modified from a geometrical formulation of the collision term to a stochastic formulation according to Lang et al. [1]. Only NN collisions were taken into account, which for the energies considered turned out to be a justified approximation. The stochastic code was then modified according to Alexander et al. [2], and the scaling of the collision rate and the flow with the number of testparticles N was checked.

We simulated an (Au,Au)-collision at projectile energies of 250 and 400 MeV per nucleon, and $b = 3$ fm over a total time of 70 fm/c. As expected, the nuclei disintegrate slightly more violently due to the additional advection, resulting in a lower nuclear density. A calculation with the additional advection alone revealed that therefore also the collision rate decreases. However, this is partly compensated by the modified scattering probability.

The figure shows the average final transverse (perpendicular to the beam) momentum versus the reduced rapidity for protons as an indicator for nuclear flow. As it turns out, in this specific simulation the flow increases by approximately 16% for the 250 MeV collision, and 5% for the 400 MeV collision, with the introduction of the new algorithm.

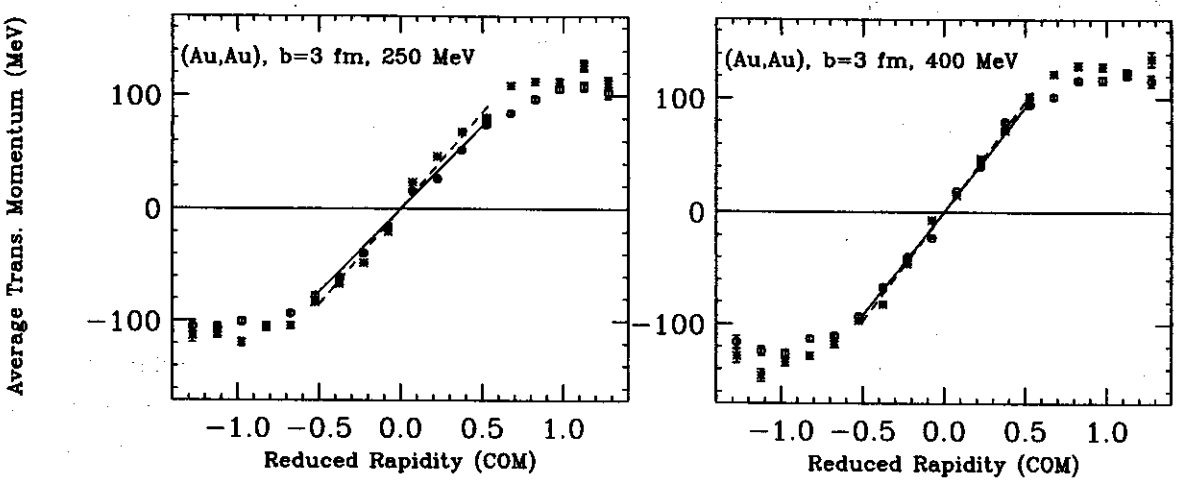

Figure 1: Average final transverse momentum versus reduced rapidity of the protons in a 250 MeV (left panel) and 400 MeV (right panel) (Au,Au) collision with $b = 3$ fm. From the slope of a linear fit around the origin, one can determine the nuclear flow. The circles and the solid fit refer to the unmodified, the stars and the dashed fit to the modified algorithm. For the 250 MeV collision, the flow is $\approx$ 147 MeV/(c·Unit of Red. Rap.) for the unmodified, and $\approx$ 170 MeV/(c·Unit of Red. Rap.) for the modified algorithm.

Introducing only the additional advection, as already pointed out, the collision rate slightly decreases, however, the nuclear flow increases by about 8% for the 250 MeV collision. With the introduction of the modified scattering probability alone, the flow increases by about 13%.

	Nuclear Flow			
Energy (MeV)	Unmodified	Modified	Plastic Ball [4]	EOS [5]
	(MeV/(c·Unit of Reduced Rapidity))			
250	132	148	130	119
400	166	185	169	151

Table 1 summarizes the results for an impact parameter averaged analysis with $b \leq 5$ fm, for both considered energies the flow increased by about 10 percent with the introduction of the modified algorithm.

CONCLUSION

Overall we found the effect of the additional advection and the modified scattering probability to be significant, but not crucial. Their implementation moves the outcome of the simulations away from the experimental results. This indicates the need for an in-medium reduction of the NN cross section. This type of reduction was first found to be needed in studies of the disappearance of flow and later also in theoretical studies based on thermodynamic T-matrix theory at finite temperature. These results were obtained by algorithm with closest approach techniques. If one wishes to address the question of the nuclear equation of state with a DSMC algorithm, however, the corrections discussed in the present paper should be taken into account.

References

1. Lang, A., Badovsky, H., Cassing, W., Mosel, U., Reusch, H.-G., and Weber, K., 1993, *J. Comp. Phys.* 106:391.

2. Alexander, F. J., Garcia, A. L., and Alder, B. J., 1995, *Phys. Rev. Lett.* 74:5212.
3. Résibois, P. M., and De Leener, M., 1977, "Classical Kinetic Theory of Fluids," p. 156*ff*, John Wiley & Sons, New York.
4. Gustafson, H. A., et al. (Plastic Ball Collaboration), 1988, *Mod. Phys. Lett. A* 3:1323.
5. Partlan, M. D., 1995, et al. (EOS Collaboration), 1995, *Phys. Rev. Lett.* 75:2100.
6. P. Danielewicz and G.F. Bertsch, *Nucl. Phys. A533*(1992), 712 (Appendix)

EXCESS ELECTRON PAIRS FROM HEAVY-ION COLLISIONS AT CERN AND A MORE COMPLETE PICTURE OF THERMAL PRODUCTION

Kevin Haglin

Dynamics of high-energy heavy-ion collisions can be probed, at least in principle, by photons and dileptons since they are produced continuously from the first moments of nuclear contact throughout the entire evolution and interact only weakly through electromagnetic coupling to the hadronic medium. Their mean free paths are many times greater than typical reaction-zone sizes allowing them to bring out valuable information on the earlier stages. Recently an intriguing report from CERN[1] brought forth results for dielectron signals observed in heavy-ion induced reactions as compared with proton-induced results. While the p+Be and p+Au data at 450 GeV were not inconsistent with estimations from hadronic decays, the S+Au results showed an enhancement by a factor of 5.0± 2.7 over hadronic decay contributions when integrated over mass from 0.2 to 1.5 GeV.

The natural conclusion drawn from these theoretical estimates and experimental data was that the excess is most probably due to $\pi\pi$ annihilation in a heated hadronic environment. But since the excess is pronounced for masses near 500 MeV and lower, this is not obviously annihilation. If not, then what? Taking the point of view to use free-space masses and widths (and including a collision broadening for ρ), I show in this report[2] that the "excess" dielectron signal is due in part due to $\pi\pi$ annihilation, but could have important contributions from pion-resonance $\pi\rho \to \pi e^+e^-$ scattering.

Consider a central collision of sulfur on gold at 200 GeV/u which will produce a "fire cylinder" of transverse radius R_T equal to that of the sulfur nucleus. Assuming isentropic expansion and relating observed rapidity densities to initial times and temperatures[3], T_i is quite high—of the order 350 MeV. Instead, if either the mixed phase (of quark and hadron coexistence) or pure plasma phase is reached, the additional degrees of freedom will effectively keep the temperature lower. Simulations of relativistic transport[4] support this picture since they are able to reproduce transverse mass spectra for both pions and protons with an initial temperature of $\sim$ 185 MeV and a finite chemical potential $\mu_\pi = 135$ MeV.

The observed spectrum of dielectrons will consist of several components, each coming from different mechanisms from different stages of the evolution. Below 150 MeV mass a nonthermal component of π^0 and η Dalitz dominates and the observed yields are consistent with estimates[1]. Hadronic radiative decays contribute to higher masses and the largest seems to be $\omega \to \pi^0 e^+e^-$ [1,5], although there are recent suggestions that partial $U(1)_A$ restoration could modify η' physics in ways relevant for this experiment[6]. Direct decay of vector mesons ρ^0 and ω will also be a strong source of pairs fairly near their free space masses. Production of a nonzero four volume of hot matter generates contribution from pion annihilation $\pi^+\pi^- \to e^+e^-$, whose strength depends on the average temperature. In this four volume there are also myriad hadronic reactions able to produce pairs. Elastic scattering of π's with ρ's is dominated by resonant a_1 formation as the average $\sqrt{s}$ for $T \sim 150$ MeV is near the centroid of the rather broad a_1 mass distribution. Since the a_1 has a radiative decay channel as well, it follows that scattering can produce real or virtual photons. For real energetic photon production, the reaction $\pi\rho \to a_1 \to \pi\gamma$ has been shown to be very important[7,8]. As $E_\gamma \to 0$ phase space shrinks to a point and this mechanism contributes nothing. Zero invariant mass for virtual photons does not require zero energy as q_0^2 and $\vec{q}^{\,2}$ could separately be very large. Consequently the amplitude for $\pi\rho \to \pi e^+e^-$ will go like $1/M^2$ for small mass. Near the rho, vector dominance takes over and the amplitude goes like $1/(M^2 - m_\rho^2 + im_\rho\Gamma_\rho)$.

More generally, the rate for producing electron pairs is related to the imaginary part of the retarted photon self-energy which, to one-loop order, corresponds to decay and annihilation. The pion-resonance scattering process being of two-loop order would require additional renormalization and the added nuisance of an additional Matsubara sum, but the prescription is clear. As the field theoretic methods are completely equivalent to kinetic theory at given order in the coupling, the latter is chosen for convenience. It builds upon evaluating tree-level Feynman diagrams and folding thermal momentum distributions with transition amplitudes to arrive at an average rate in medium for a given process. The dominant contribution to $\pi\rho \to \pi e^+ e^-$ proceeds through the a_1 resonant and includes a vector-dominance form factor whose width is taken to be a function of temperature to include collision broadening. It is computed just as in Ref. [9] but including finite pion chemical potential and then parametrized for 100 $< T <$ 200 MeV by

$$\Gamma_\rho(T) \;=\; \Gamma_\rho + \left[a + bT + cT^2\right] \tag{1}$$

where Γ_ρ is the free space width and $a = 0.50$ GeV, $b = -7.16$ and $c = 30.16$ GeV^{-1}.

An effective lagrangian for axial-vector–vector–pseudoscalar interaction is chosen for simplicity to be the following[7]

$$L_{AV\phi} \;=\; g_{AV\phi} A_\mu \left[(p_\phi \cdot p_V) g^{\mu\nu} - p_\phi^\nu p_V^\mu\right] V_\nu \tag{2}$$

where A, V, and ϕ are respectively, axial-vector, vector and pseudoscalar fields. A treatment of this interaction from a chiral lagrangian approach has yielded results for photon production roughly consistent with those from this less complicated parametrization[7,8]. The coupling constant is adjusted to give a decay $\Gamma_{a_1 \to \pi\rho} = 400$ MeV[10] to match the Particle Data Group[11] value and the coupling of a_1 to π and γ is then taken to be the vector-dominance value of $g_{a_1\pi\rho}(e/f_\rho)$, where f_ρ is the coupling of rho to pions. Numerically these turn out to be $g_{a_1\pi\rho} = 16.1$ GeV^{-1} and $g_{a_1\pi\gamma} = 0.81$ GeV^{-1} for $m_{a_1} = 1230$ MeV.

The invariant rate for thermally producing a lepton pair of mass M and individual three momenta $\vec{\ell}_+$ and $\vec{\ell}_-$ via the process $\rho(p_a) + \pi(p_b) \to \pi(p_1) + \ell_+ \ell_-$ can be written generally as

$$E_+ E_- \frac{dN}{d^4x\, dM^2\, d^3\ell_+\, d^3\ell_-} \;=\; \frac{\mathcal{N}}{4(2\pi)^2} d\omega_a\, d\omega_b\, d\omega_1 f(E_a) f(E_b) \tilde{f}(E_1) |\overline{\mathcal{M}}|^2$$

$$\times \delta^4(p_a + p_b - p_1 - \ell_+ - \ell_-)\, \delta\left[(\ell_+ + \ell_-)^2 - M^2\right] \tag{3}$$

where $\mathcal{N}$ is an overall degeneracy factor, $d\omega_a = d^3p_a/[(2\pi)^3 2E_a]$ and so on, f is the Bose-Einstein distribution, $\tilde{f} = 1 + f$ to account for medium (Bose) enhancements and $|\overline{\mathcal{M}}|^2$ is the initial spin averaged and final spin summed squared matrix element. Integration over the full individual lepton three momenta can be additionally performed to arrive at the total rate for given mass. However, the differential rate is more useful here since limited transverse momentum and rapidity ranges can then be integrated to approximate experimental configurations.

First, we set the pion chemical potential to zero and compute the rates shown in Fig. 1a for $\pi\pi$ annihilation as compared with $\pi\rho \to \pi e^+ e^-$. Formulas for annihilation are not shown because they are by now textbook expressions[12] and have been recently used in a similar study[13]. For additional comparison we show also an estimate of pion scattering with bremsstrahlung[14]. All three contributions become roughly the same around 350 MeV mass, which is the lower end of the window of the observed excess over hadronic decays.

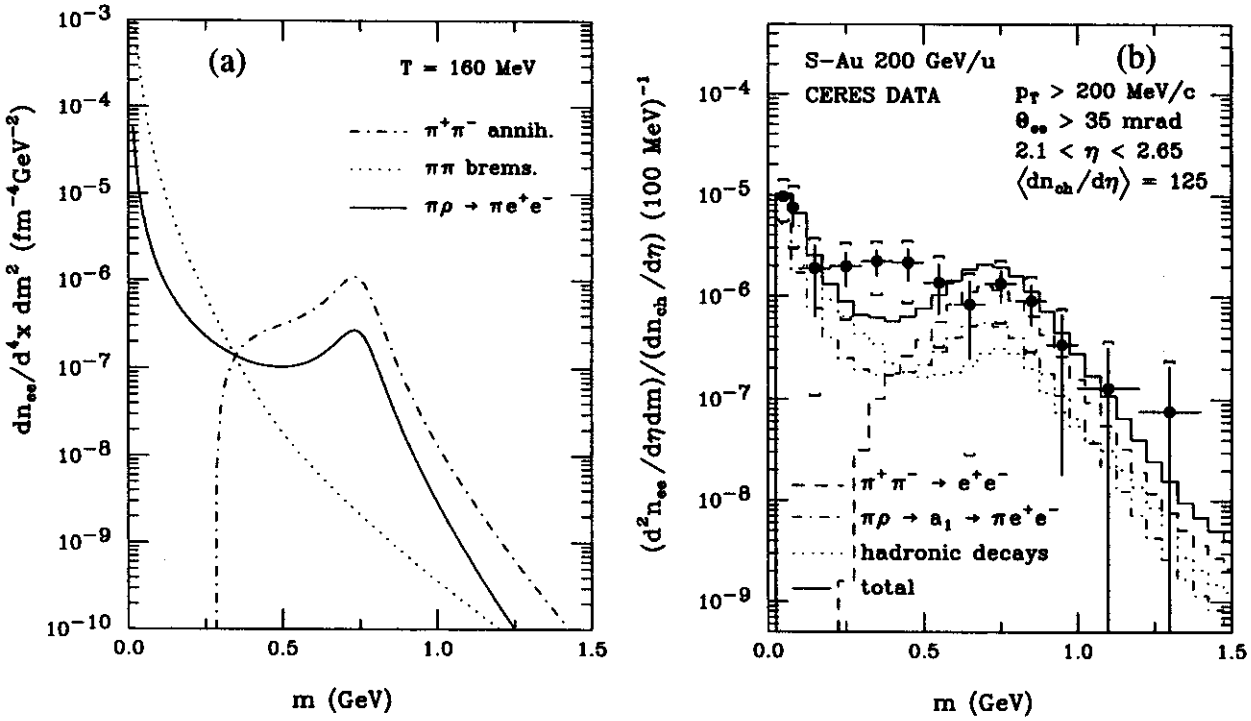

Fig. 1: Thermal rate for producing electron pairs (a) at $T = 160$ MeV for the process $(\pi\rho \to \pi e^+e^-)$ in the solid curve, pion bremsstrahlung in dotted curve and $\pi\pi$ annihilation in the dashed curve; and (b), lepton pair yields observed in experiment as compared with pion+resonance scattering $(\pi + \rho \to \pi e^+e^-)$ in the dot-dashed distribution, estimated hadronic decays through event generation taken from Ref. [1] (dotted), $\pi\pi$ annihilation in the (dashed) and with the sum of annihilation, scattering and decays (solid).

In order to compare with experiment an integration of these rates over a spacetime evolution must be preformed. We assume a Bjorken model[15] and neglect any transverse flow effects. Choice of specific times or temperatures must be made. Here we take $T_i = 188$ MeV, $T_c = 160$ MeV, $T_f = 140$ MeV and $\mu_\pi = 135$ MeV. The rho is again assigned a collision broadened width. Total yield is the sum of contributions from the mixed plus cooling phases[16]. Written out in detail, it is

$$\frac{dN}{dy\,dM} = \frac{\pi R_T^2}{2}\left(\frac{T_i}{T_c}\right)^6 \tau_i^2 r(r-1)\int \frac{d^3\ell_+}{E_+}\frac{d^3\ell_-}{E_-}\left[E_+E_-\frac{dN}{d^4x\,dM\,d^3\ell_+ d^3\ell_-}(T=T_c)\right]$$

$$+3\pi R_T^2 T_i^6 \tau_i^2 r^2 \int_{T_f}^{T_c}\frac{dT}{T^7}\frac{d^3\ell_+}{E_+}\frac{d^3\ell_-}{E_-}\left[E_+E_-\frac{dN}{d^4x\,dM\,d^3\ell_+ d^3\ell_-}\right], \qquad (4)$$

where r is the ratio of degrees of freedom in QGP phase to that of hadron phase and is ~ 12. The pseudorapidity density will be assumed to be equal to the rapidity density $dN/dydM \approx dN/d\eta dM$.

Attempting to resemble the experiment as closely as possible lepton transverse momentum integrations are limited to $p_T > 200$ MeV/c and pseudorapidities by $2.1 < \eta < 2.65$. There is also a cut in the experiment on angular separation for the pairs $\Theta > 35$ mrad to avoid resolution difficulties. We ignore this limitation here as it should only have small influence on the result for masses greater than 200 MeV. Finally, we normalize just as in the experiment by dividing the yield $d^2N/d\eta\,dM$ by the average charged particle pseudorapidity density $\langle dN_{\rm charged}/d\eta\rangle = 125$.

Partial and total yield estimates are shown in Fig. 1b as dashed ($\pi\pi$ annihilation), dot-dashed ($\pi\rho$ scattering), dotted (hadronic decays as presented in Ref.[1]) and solid (total of annihilation, scattering and decays). Inclusion of the a_1 seems to account for part of the excess but still leaves the door open for other possibilities. Additional pairs could be coming from $\pi\pi \to \rho\gamma^*$ and $\pi\pi \to \pi\gamma^*$[17]. They could also be coming from decays not already considered and possibly even a bremsstrahlung component[18].

As a brief summary, I have pointed out that the recently observed dielectron signal being in excess of hadronic decays in S+Au collisions at 200 GeV/u is likely coming not only from $\pi\pi$ annihilation as was suggested, but could also be partly due to pion plus resonance $\pi\rho \to \pi e^+e^-$ scattering. The picture emerging for thermal production of low-mass dielectrons becomes richer and more challenging as it calls for next-to-leading order treatments of the photon self-energy.

References

1. G. Agakichiev *et al.*, Phys. Rev. Lett. 75, 1272 (1995).
2. K. L. Haglin, Phys. Rev. C, in press.
3. R. Hwa and K. Kajantie, Phys. Rev. D 32, 1109 (1985).
4. G. Q. Li, C. M. Ko and G. E. Brown, Phys. Rev. Lett. 75 4007 (1995).
5. C. Gale and P. Lichard, Phys. Rev. D 49, 3338 (1994).
6. J. Kapusta, D. Kharzeev and L. McLerran, hep-ph/9507343.
7. L. Xiong, E. Shuryak and G. E. Brown, Phys. Rev. D 46, 3798 (1992).
8. C. Song, Phys. Rev. C 47, 2861 (1993).
9. K. Haglin, Nucl. Phys. A 584, 719 (1995).
10. K. Haglin, Phys. Rev. C 50, 1688 (1994).
11. Review of Particle Properties, Phys. Rev. D 45-II (1992).
12. C.-Y. Wong, *Introduction to High-Energy Heavy-Ion Collisions*, World Scientific, pg. 332 (1994).
13. D. K. Srivastava, B. Sinha and C. Gale, Phys. Rev. C 53 R567 (1996).
14. K. Haglin, C. Gale and V. Emel'yanov, Phys. Rev D 46, 4082 (1992); Phys. Rev. D 47, 973 (1993).
15. J. D. Bjorken, Phys. Rev. D 27, 140 (1983).
16. K. Kajantie *et al.*, Phys. Rev. D 34, 2746 (1986).
17. K. Haglin, Talk given at the INT/RHIC Workshop "Electromagnetic Probes of Quark Gluon Plasma", INT, Seattle 24–27 January 1996.
18. D. Pal, K. Haglin and D. K. Srivastava, Phys. Rev. C, in press.

FINITE Δ LIFETIME EFFECTS ON BREMSSTRAHLUNG FROM INELASTIC NUCLEON-NUCLEON REACTIONS

Kevin Haglin

Reaction channels involving hadronic inelasticities have been shown to be quite important for lepton pair production in 5 GeV nucleon-nucleon collisions[1] and relatively important for energies as low as 1 GeV[2]—particularly for understanding the ratios of yields in pd/pp reactions as a function of mass when the beam energy increases from 1 to 5 GeV. For 5 GeV protons it was found that simple virtual bremsstrahlung in pp scattering was larger than from pn. This is remarkable since the reverse is clearly true for low energy reactions where the dipole limit is realized and destructive interference nearly completely suppresses pp bremsstrahlung. Still, it is reasonable that at some energy the interference becomes less important and since the proton-proton configuration consists of four "antennae" for radiation while the proton-neutron case has only two, pp might be larger. Given this, a pp/pn ratio of 2 is not unreasonable.

It was also shown that these simple bremsstrahlung contributions were an order of magnitude below the low-mass experimental data from the Dilepton Spectrometer (DLS) at Lawrence Berkeley Laboratory for 4.9 GeV pd and pp reactions[3]. The missing strength seems to be coming from η-Dalitz decays, Δ radiative decays and many-body bremsstrahlung. The accuracy of calculations for radiative decays is unfortunately limited by relatively large uncertainties in η and Δ production cross sections. On the other hand, data for the pion production cross sections are quite good and ought to be used to refine those many-body bremsstrahlung calculations. The method previously used to treat them was perhaps not totally satisfactory since it neglected the finite lifetime of the Δ resonances which are primarily responsible for producing the final-state pions.

In a description of "soft" radiative emission the dominant contributions originate from the photon being produced by the external legs. Half off-shell hadrons in each case propagate in such a way that they become "scalar-like" in the soft limit—this is essentially the result of Low's theorem[9]. The invariant amplitude for lepton pair radiation can be written as

$$\mathcal{M} \;=\; e\mathcal{M}_0\, J\cdot L \tag{1}$$

where e is the fundamental charge, $\mathcal{M}_0$ is the corresponding nonradiative amplitude for the process $a+b\to 1+\ldots+n$, J^μ is the hadronic electromagnetic current and $L^\mu = (e/M^2)\bar{u}(p_-,s_-)\gamma^\mu v(p_+,s_+)$. In other words, the on-shell hadronic physics factorizes from the electrodynamic influences in this soft photon approximation. If the invariant mass of the lepton pair is M, the absolute square of the matrix element summed over final spins and averaged over initial ones is

$$|\overline{\mathcal{M}}|^2 \;=\; 4\pi\alpha\,|\overline{\mathcal{M}_0}|^2\, J^{\mu\nu}\, L_{\mu\nu} \tag{2}$$

where $L^{\mu\nu} = 8\pi\alpha/M^4\left[q^\mu q^\nu - \ell^\mu\ell^\nu - g^{\mu\nu}M^2\right]$, $q = p_+ + p_-$ and $\ell = p_+ - p_-$. Then the fully covariant cross section for producing an e^+e^- pair of mass M is

$$d\sigma \;=\; \frac{\alpha^2}{8\pi^4 M^2}\int d\sigma_0\left[-J^2 - \frac{1}{M^2}(\ell\cdot J)^2\right]\frac{d^3p_+}{E_+}\frac{d^3p_-}{E_-}. \tag{3}$$

Upon obtaining Eq. (3) the four-momentum q of the photon was neglected in the overall energy-conserving delta function. To partially restore proper energy conservation we multiply by the ratio $\Phi = R_n(s-2\sqrt{s}q_0+M^2)/R_n(s)$. The function R_n, being n-body phase space, effectively shrinks the momentum space over which Eq. (3) is to be integrated so it is nearer to the physical one. Then, after integrating over lepton solid angles in the dilepton rest frame, the differential cross section can be written[10]

$$q_0\frac{d\sigma}{d^3qdM^2} = \frac{\alpha^2}{12\pi^3M^2}\int -J^2\,d\sigma_0\,\Phi. \tag{4}$$

Equation (4) can now be integrated over the available dilepton three momentum which is governed by Φ in order to obtain an approximate mass distribution.

In Ref. [1] the one, two and three pion final states were studied. It was argued that pions were primarily produced through excitation and subsequent decay of deltas. The nonradiative matrix elements were chosen to reflect the presence of deltas but the electromagnetic current did not include the Δ's finite lifetime. In short, the pions in this approach appear instantly and therefore have a very large effective acceleration. In reality they appear on average 1.6 fm/c after excitation and thus have a softer acceleration. We might say therefore, that Ref. [1] provided an upper limit to these contributions since time delaying the appearance of the pions would weaken the ensuing radiation. Here we propose a gauge-invariant amplitude for inelasticities which includes the finite width of the Δ. For instance, consider the nonradiative reaction $p(p_a)+p(p_b)\to n(p_1)+p(p_2)+\pi^+(p_3)$. There are two dominant ways in which this proceeds: $p+p\to n+\Delta^{++}\to n+p+\pi^+$ and $p+p\to p+\Delta^+\to p+n+\pi^+$. Define $\mathcal{M}_0^{++}$ ($\mathcal{M}_0^{+}$) as the nonradiative amplitude that proceeds through the Δ^{++} (Δ^+) excitation. Let us take the full, dilepton emission amplitude—which replaces Eq. (1) and therefore results in a slightly different expression for the invariant cross section as compared with Eq. (4)—to be the following

$$\mathcal{M} = e\left[\mathcal{M}_0^{++}J^\mu_{++}+\mathcal{M}_0^{+}J^\mu_{+}\right]L_\mu \tag{5}$$

where the two different currents are

$$\begin{aligned}
J^\mu_{++} &= -Q_a\frac{p_a^\mu}{p_a\cdot q}-Q_b\frac{p_b^\mu}{p_b\cdot q}+Q_1\frac{p_1^\mu}{p_1\cdot q}\\
&\quad+(Q_2+Q_3)\left[\frac{2(p_2+p_3)^\mu}{(p_2+p_3+q)^2-m_\Delta^2-im_\Delta\Gamma_\Delta(m_{23})}\right]\\
&\quad+Q_2\frac{p_2^\mu}{p_2\cdot q}\left[\frac{(p_2+p_3)^2-m_\Delta^2-im_\Delta\Gamma_\Delta(m_{23})}{(p_2+p_3+q)^2-m_\Delta^2-im_\Delta\Gamma_\Delta(m_{23})}\right]\\
&\quad+Q_3\frac{p_3^\mu}{p_3\cdot q}\left[\frac{(p_2+p_3)^2-m_\Delta^2-im_\Delta\Gamma_\Delta(m_{23})}{(p_2+p_3+q)^2-m_\Delta^2-im_\Delta\Gamma_\Delta(m_{23})}\right]\\
J^\mu_{+} &= -Q_a\frac{p_a^\mu}{p_a\cdot q}-Q_b\frac{p_b^\mu}{p_b\cdot q}+Q_2\frac{p_2^\mu}{p_2\cdot q}\\
&\quad+(Q_1+Q_3)\frac{2(p_1+p_3)^\mu}{(p_1+p_3+q)^2-m_\Delta^2-im_\Delta\Gamma_\Delta(m_{13})}
\end{aligned}$$

$$+Q_1 \frac{p_1^\mu}{p_1 \cdot q} \left[\frac{(p_1+p_3)^2 - m_\Delta^2 - i m_\Delta \Gamma_\Delta(m_{13})}{(p_1+p_3+q)^2 - m_\Delta^2 - i m_\Delta \Gamma_\Delta(m_{13})} \right]$$

$$+Q_3 \frac{p_3^\mu}{p_3 \cdot q} \left[\frac{(p_1+p_3)^2 - m_\Delta^2 - i m_\Delta \Gamma_\Delta(m_{13})}{(p_1+p_3+q)^2 - m_\Delta^2 - i m_\Delta \Gamma_\Delta(m_{13})} \right], \tag{6}$$

with the Q's being particle charges in units of proton charge, $m_{23}^2 = (p_2+p_3)^2$ and $m_{13}^2 = (p_1+p_3)^2$ being the squared invariant masses. The energy dependence of the delta width is known to go like the cube of the center-of-mass momentum of the decay products (pion and nucleon) and normalization is taken to give $\Gamma_\Delta(m_\Delta) = 120$ MeV for $m_\Delta = 1232$ MeV. Considering the width instead as a parameter and the limit $\Gamma_\Delta(\omega) \to \infty$, the terms in which radiation originates from the Δs disappear while the remaining radiation reduces to precisely the current for reactions involving stable hadrons. This amplitude of Eq. (5) includes radiation off all external legs of the diagrams and "time-delays" the pion by the lifetime of the Δ just as would come out of a diagrammatic calculation. While it neglects all diagrams with four-point or contact vertices, these are subleading order in the soft photon approximation anyway.

Although the influence of the finite width of the delta in the electromagnetic current is reaction dependent, we can get an idea of the relative importance by considering a single channel and then conjecture that it is roughly of the same strength in the others. So in Fig. 1 we plot the results for

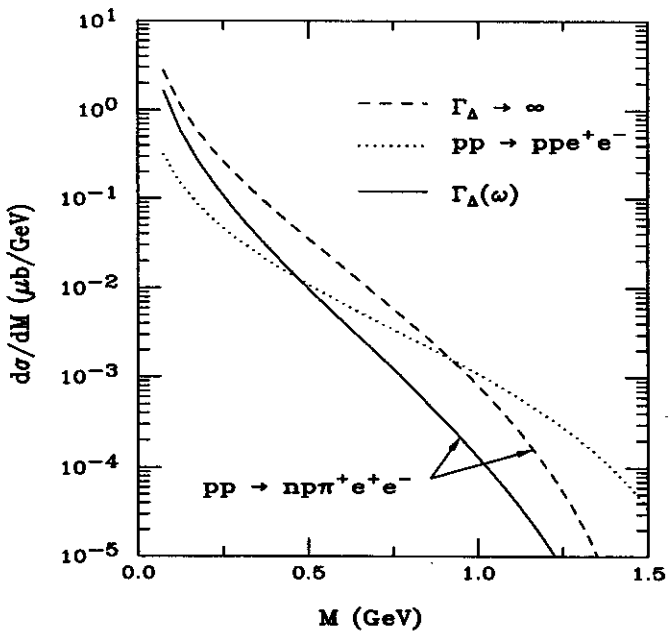

Fig. 1: Cross section for dielectron emission in 4.9 GeV proton-proton bremsstrahlung (dotted curve), $pp \to np\pi^+e^+e^-$ with an infinitely broad Δ in the electromagnetic (EM) current (dashed curve) and with a realistic energy-dependent width Γ_Δ in the EM current (solid curve).

simple $pp \to ppe^+e^-$ bremsstrahlung as compared with $pp \to np\pi^+e^+e^-$ for two cases of Γ_Δ: first an infinitely broad delta is considered $\Gamma_\Delta \to \infty$ which reproduces what was done in Ref. [1] and second, an energy dependent width is taken. Note that simple bremsstrahlung is nearly an order of magnitude below the inelastic channel's contribution at low mass. Separate studies of the beam energy dependence seem to indicate that already at 1 GeV bremsstrahlung these hadronically inelastic channels compete

with simple bremsstrahlung, while they are clearly more important in the low mass region as energy increases to 5 GeV[2]. Using a current with "instantly produced pions" as compared with a current which uses "time-delayed pions", the duration of which depends on the Δ width, results in less than a factor of 2 suppression at low mass. This indicates that one can be relatively satisfied with the size of previous estimates for hadronic inelasticities' contribution to e^+e^- emission.

References

1. K. Haglin and C. Gale, Phys. Rev. C 49 (1994) 401.
2. K. Haglin, "Dilepton production in proton+nucleon collisions", 9th High-Energy Heavy-Ion Study, Lawrence Berkeley Laboratory Report Number LBL-35984 (1993) 11.
3. H. Z. Huang *et al.*, Phys. Rev. C 39 (1994) 314.
4. K. L. Haglin, Ann. Phys. 212 (1991) 84.
5. K. Haglin, J. Kapusta and C. Gale, Phys. Lett. B224 (1989) 433.
6. M. Schäfer *et al.*, Phys. Lett. B221 (1989) 1.
7. M. Schäfer *et al.*, Nucl. Phys. A 575 (1994) 429.
8. M. Jetter and H. W. Fearing, Phys. Rev. C 51 (1995) 1666.
9. F. E. Low, Phys. Rev. 110 (1958) 974.
10. P. Lichard, Phys. Rev. D 51 (1995) 6017.

GAUSSIAN WAVE-PACKET DYNAMICS WITH AND WITHOUT CORRELATIONS

Dieter Kiderlen and Pawel Danielewicz

Given difficulties in the theoretical description of heavy-ion collisions at intermediate beam energies (10 MeV $\lesssim E/A \lesssim$ 150 MeV), with the dynamics of intermediate-mass fragment production, fluctuations, instabilities, quantal effects, and so on, the quantum molecular model [1] (termed FMD) was met with quite some expectations. In this model, the quantal wave function for a reacting system is represented as a product of the Gaussian wave-packets for individual nucleons. These packets have dynamic centers, phases, and widths obeying equations of motion following from a variational principle. In this work we investigate the fragment production within an FMD type model.

Careful examination of the FMD model [1] reveals from an outset a specific problem concerning the fragment emission. Thus, inside a fragment, the constituent nucleons are localized in the relative separations. When the wave function is a product of single-particle wave functions, this implies a localization of the fragment center of mass. While low-energy nucleons escaping from a larger residue become delocalized [2], getting rid of the kinetic energy associated with the localization, this cannot be the case for the fragments. The c.m. localization energies, e.g. in the range of $A = (2\text{–}4)$ nuclei, are within (10–30) MeV and, given that the temperatures in excited nuclei in reactions could be as low as (5–10) MeV, these energies could result in significant thermal penalty-factors for fragment emission, $e^{-\Delta E/T}$.

Correspondingly, we investigated fragment production within a model that generalizes [1], where the wave function, of a gaussian form, allows for correlations between the nucleons within fragments:

$$\langle \boldsymbol{x}_1, \ldots, \boldsymbol{x}_N | \Psi \rangle = \mathcal{N} \exp\Big(- A_{ij} (\boldsymbol{x}_i - \boldsymbol{r}_i) \cdot (\boldsymbol{x}_j - \boldsymbol{r}_j) + i \boldsymbol{p}_i \boldsymbol{x}_i \Big) \chi \,. \tag{1}$$

Here χ is a normalized spin-isospin wave function, $\boldsymbol{x}_i$ denotes position vector of particle i, and the norm is $\mathcal{N} = (\det(2\,\mathrm{Re}A)/\pi^N)^{3/4}$ for N particles. The parameters of the spatial wave function, which depend on time, include the elements of the width matrix A, as well as the centroids $\{\boldsymbol{r}_i\}$ and momenta $\{\boldsymbol{p}_i\}$ of each particle. At present, the wave function is not antisymmetrized, only a Pauli pseudopotential is used. The form (1) includes the special case of the width diagonal in particle indices, $A_{ij} = \delta_{ij} A_i$. The wave function reduces then to a product of single-nucleon wave functions such as utilized in the FMD [1,2], EQMD [3], AMD [4] and QMD [5] calculations (for the latter two, the width is no dynamic variable.).

On writing the time-dependent variational principle in the form $\delta \int_{t_1}^{t_2} \mathcal{L}\, dt = 0$, with the Lagrange function $\mathcal{L} = \langle \Psi | i\hbar \frac{d}{dt} - H | \Psi \rangle$ the equations of motion for the parameters follow as Lagrange-Euler equations. The equations for the centroids and momenta can be written in the Hamilton's form with the expectation value of the Hamilton operator playing the role of the classical Hamiltonian,

$$\dot{\boldsymbol{r}}_i = \partial \langle H \rangle / \partial \boldsymbol{p}_i \,, \qquad \dot{\boldsymbol{p}}_i = -\partial \langle H \rangle / \partial \boldsymbol{r}_i \,. \tag{2}$$

The elements of the width matrix satisfy

$$\frac{d}{dt}\,\mathrm{Re}A_{ij} = \sum_{m \le n} \mathcal{B}^{-1}_{\frac{i(i-1)}{2}+j,\,\frac{n(n-1)}{2}+m} \frac{\partial \langle H \rangle}{\partial \mathrm{Im}A_{nm}} \,, \qquad \frac{d}{dt}\,\mathrm{Im}A = -\mathcal{B}^{-1}\,\frac{\partial \langle H \rangle}{\partial \mathrm{Re}A} \,, \tag{3}$$

where B is defined by

$$B^{-1}_{\frac{n(n-1)}{2}+m,\frac{i(i-1)}{2}+j} = \frac{2}{3}\left(\mathrm{Re}A_{ni}\mathrm{Re}A_{mj} + \mathrm{Re}A_{nj}\mathrm{Re}A_{mi}\right), \tag{4}$$

with $1 \le m \le n \le N$, $1 \le j \le i \le N$. The indices in the second equation in (3) should be handled in the same manner as in the first of the equations where they are written out explicitly.

To make the calculation of the expectation value of the Hamiltonian, as well as its derivatives, analytic, we choose the internucleon potential of such a form as in [2],

$$V = \sum_k u_k \sum_{i<j} \left(w_k + (1-w_k)P^M_{ij}\right) \exp\left(-\lambda_k^{-2}(\boldsymbol{x}_i - \boldsymbol{x}_j)^2\right), \tag{5}$$

where P^M_{ij} is the Majorana operator exchanging spatial coordinates of the particles i and j. The sum over k extends over the repulsive and attractive contributions to the potential. The values for u_k, λ_k and w_k are listed in [2].

The trial wave functions should, generally, be antisymmetrized. When the width matrix A is though not diagonal in particle indices, then the wave function is not a product of single-particle wave functions and, at present, the antisymmetrization is not feasible for the particle number greater than ~ 16. Respectively, we resort to the Pauli potential to simulate the effects of antisymmetrization. The potential acts only between particles of the same spin and isospin and we choose it proportional to the Majorana operator, $V_{Pauli} = \sum_{ij} u_3 P^M_{ij}$. That is motivated by the fact that the expectation value of P^M_{ij} for the product wave function is equal to the square of the scalar product of the wave functions $\psi_{i,j}$ for the two particles, $\langle P^M_{ij}\rangle = |\langle\psi_i|\psi_j\rangle|^2$. When one wave function approaches another, the system reacts with a repulsive force. The Pauli potential is added as a third component to (5) ($w_3 = 0$, $\lambda_3^{-1} = 0$), and the value of u_3 is adjusted to best fit the properties of ground-state nuclei. Unfortunately, such u_3 depends quite significantly on the mass. Using parameter set $B1$ from [2] (originally from [6]) in (5), we obtain e.g. optimal $u_3 = 70$ MeV for $A = 12$ and $u_3 = 200$ MeV for $A = 80$.

Since we do not antisymmetrize the wave function, we first explore situations where antisymmetrization plays a secondary role. This should be the case when a highly excited system formed in the central heavy-ion collision decays into vacuum. We assume that the internal degrees of freedom are, generally, equilibrated, and only allow for the variable strength of the radial flow.

To simulate the system, we distribute centroids randomly within a spatial volume of radius R and in the momentum according to the finite-temperature Fermi distribution. To account for the flow, we add to the momentum of each particle a component proportional to the position vector relative to the overall center of mass. The proportionality constant determines the amount of flow energy in the initial state. The width matrix is initialized as a real multiple of the unit matrix. An example of such an initial state is shown in Fig. 1a. In the particular case $A = 80$, $R \simeq 5$ fm, and rms radii of individual packets are equal to 1.9 fm.

The time evolution for the initial state specified above, depends on whether the width matrix is allowed to change with time or not. For the dynamic matrix, whether or not restricted to the diagonal form, the system emits, in the course of time, a number of single nucleons. This number generally increases with the energy of the system. However, at no particular energy, emission of IMF or even α particles is observed. This appears to be true irrespective of how we divide the excitation energy into collective and

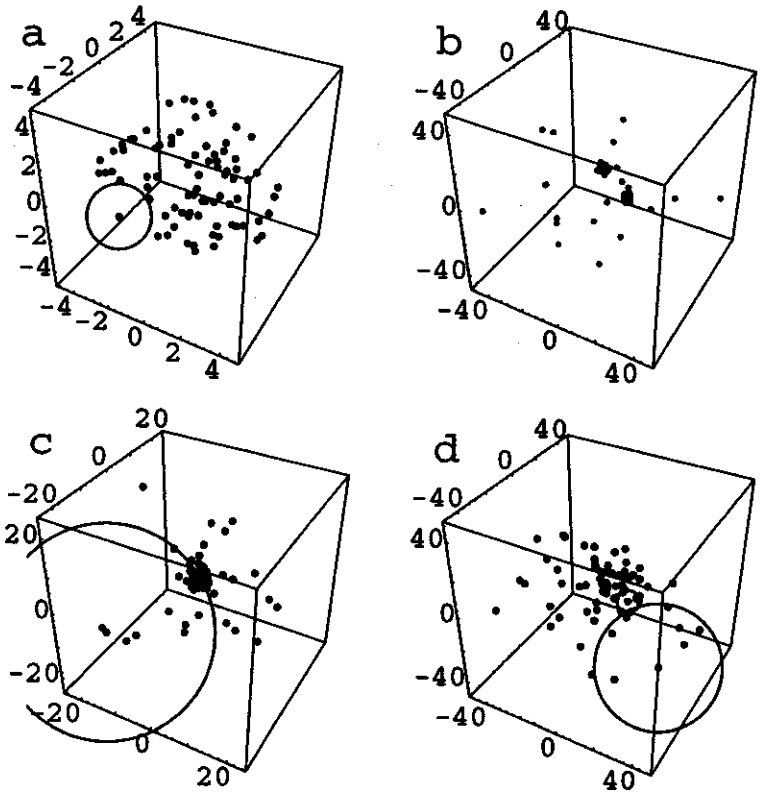

Figure 1: Particle centroids (dots) in the configuration space for $A = 80$, in the initial state (a) and at $t = 200$ fm/c for the static wave-packet width (b), and for the dynamic width matrix (c) and (d). In (c), the initial flow energy is lowered, compared to (b) and (d), by the initial energy content in the localization of the wave packets. The circles indicate rms radii of the most and least localized Gaussians. The radii of the packets in the case (b), and the radii of the most localized packets in the case (d), are equal to the radii of the dots representing centroids. The axes show distances in fm.

thermal. Examples of the late-stage distributions of centroids in space are given in Figs. 1(d) and 1(c), respectively, for the initial excitation energy of 26 and 14 MeV/nucleon. For the particular initial state, the centroid distributions at the respective time are not distinguishable by eye between the cases with and without correlations. While some centroids appear to be close to each other in the figures, at some distance from the main residue, the respective wave-packet widths are so large that, at $t = 300$ fm/c, all relative energies of the emitted particles are positive.

The situation is qualitatively different in the case of a static width. Thus, Fig. 1(b) shows centroids for the system evolved using a static width, from the initial state shown in Fig. 1(a), for the same available energy (given the frozen width) as the system in Fig. 1(d). In Fig. 1(b) two IMF's as well as two dinucleons are seen and they will remain stable. Additional clusters were emitted before $t = 300$ fm/c and have left the displayed spatial region. When experimenting with the case of dynamical width, we attempted to slow down the width evolution. We have found that this evolution needs to be slowed down by a factor of (5–10) in order to observe the cluster formation.

The lack of cluster formation for the dynamic width matrix seems to be in contradiction with the results of FMD [2]. A closer examination, however, indicates that the clusters seen in final states of FMD calculations [2] were not formed during the collision, but were present in the initial state and survived the

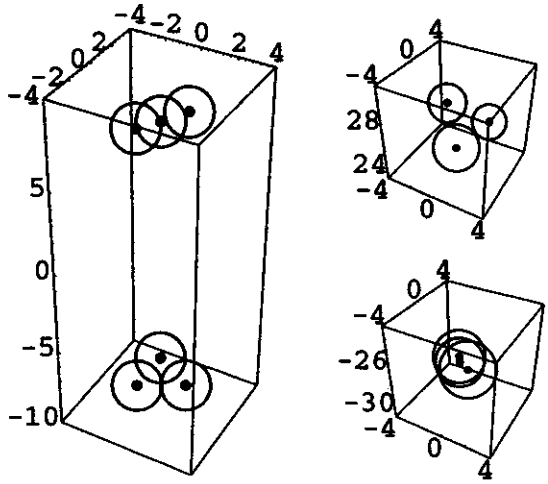

Figure 2: $^{12}C + ^{12}C$ collision at 29 MeV/nucleon: initial (left) and late ($t = 300$fm; right) states. The beam axis is directed vertically. The axes show distances in fm.

collision. To investigate the particular issue, we simulated symmetric collisions of different nuclei. Given the potential (5) and our choice of the Pauli potential, the centroids within the ground state of ^{12}C form three α-type clusters of four nucleons each. On the other hand, within ^{40}Ca the centroids of individual nucleons situate themselves at the center of the overall mass position; the widths for different nucleons take on different values. Thus, when considering the $^{12}C + ^{12}C$ collision, we deal with six sub-clusters in initial state, and with none in the $^{40}Ca + ^{40}Ca$ case.

Figure 2 shows the initial and late states of an examplary $^{12}C + ^{12}C$ collision at the beam energy of 29 MeV/nucleon. While one nucleus became highly excited in the reaction, the other has fragmented into three α particles. Each of the α particles is excited, but remaining below the threshold for particle emission. For the $^{40}Ca + ^{40}Ca$ collision with no sub-clusters in the initial state we find only a residue and some single nucleons, but no clusters in the exit channel.

The presented examples are typical ones: for none of the studied initial states, we have observed, for the dynamic width, the emission of IMF's or α particles that were not present in the initial state. This has been the case whether we included or excluded the correlations. As a general reason for the absence of cluster formation for the dynamic width, we find that, at times when the system reaches a density when clusters are expected to form, the width of the wave packets has grown so large that the interaction between different wave packets is too weak to force the width of these packets to shrink, and their centroids to approach each other sufficiently enough to form a nucleus (see also Chomaz et al. [7]).

The values of the widths are not necessarily unphysically large, as nucleons are expected to get delocalized with the reaction progress. In reality, though, while broad wave packets of different nucleons overlap in space, the interaction between the nucleons should be generally able to clump two or more nucleons, within a distance comparable to the interaction range, into a cluster. The wave function in terms of broadened Gaussians does not allow for that.

To conclude, we find that the quantal molecular dynamics in terms of Gaussian packets with a dynamic width does not allow for the production of other clusters than those present in the structure of the initial nuclei. The inclusion of long-range correlations in the Gaussian parametrization of the system

wave-function does not improve the situation. For a succesful description of fragmentation, the wave function must have a flexibility to change over a distance comparable to the interaction range. A possible way out is to keep the wave-packet width as static and to account for the spreading using a stochastic decision process. This can be nominally derived by the reduction of the wave function space to the one spanned by wave packets of constant width, which causes the appearance of a residual force associated with the kinetic-energy part of the hamiltonian.

References

1. H. Feldmeier, Nucl. Phys. A515, 147 (1990)
2. H. Feldmeier, K. Bieler and J. Schnack, Nucl. Phys. A586, 493 (1995)
3. T. Maruyama, K. Niita and A. Iwamoto, Phys. Rev. C53, 297 (1996)
4. A. Ono, H. Horiuchi, T. Maruyama and A. Ohnishi, Phys. Rev. Lett. 68, 2898 (1992)
5. J. Aichelin and H. Stöcker, Phys. Lett. B176, 14 (1986)
6. D. M. Brink and E. Boecker, Nucl. Phys. A91,1 (1967)
7. P. Chomaz et al., Talk at the 12^{th} winter workshop on nuclear dynamics, Snowbird, 1996

PARTONS IN PHASE SPACE

David A. Brown and Pawel Danielewicz

Primary hadronic collisions in a typical nuclear collision at RHIC will occur at $\sqrt{s} \sim 200A$ GeV and in regions where hadronic densities exceed the inverse volume of a typical hadron. At these energy scales, the appropriate description of a free hadron–hadron collision is in terms of the underlying partonic (quark and gluon) degrees of freedom. The cross section of such a collision is a convolution of the momentum space density of the interacting partons (the Parton Distribution Functions or PDF's) with the partonic cross section. In the high density regions of a nuclear collision, this simple momentum space theory will no longer work: a virtual parton produced in one interaction will rescatter many times before leaving the collision region. Thus, to describe a nuclear collision, we must know how the virtual partons are distributed in space as well as momentum and we must understand the space–time structure of virtual parton interactions. To incorporate the virtual partons into a model, we turn to a model such as Geiger's Parton Cascade Model [1]. This and other parton cascade models rely on initial phase–space PDF's derived using ad–hoc assumptions such as the assumption that the parton momentum and space distributions are uncorrelated. As a first step toward the complete set of phase–space PDF's for a hadron, we consider the Effective Photon Distribution of a point charge [4]. This is not just a toy model: if we ignore parton multiplication (i.e. $g \rightarrow gg$ and $g \rightarrow q\bar{q}$), the gluon PDF of a bare quark is essentially the Effective Photon Distribution of a point charge [2, 3]. With the methods we developed to find the Effective Photon Distribution, we can also study collisions of virtual partons in phase–space such as $\gamma\gamma \rightarrow e\bar{e}$. Additionally, by cutting the diagrams for $\gamma\gamma \rightarrow e\bar{e}$, we can gain insight into the parton splitting process $\gamma \rightarrow e\bar{e}$.

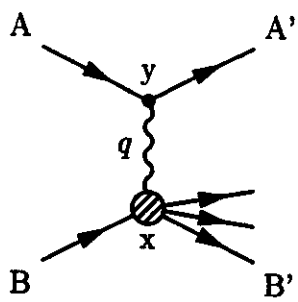

Figure 1: Generic one photon exchange process

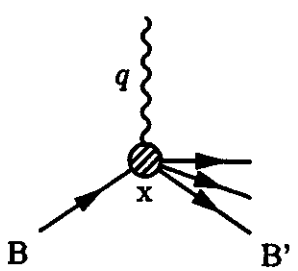

Figure 2: Generic one photon absorption process

We derive the Effective Photon Distribution by taking the absolute square of the S–matrix for the

generic one photon exchange process shown in figure 1 and rewriting it in terms of Wigner transformed currents and propagators [5, 6].

$$|S_{\mathrm{AB}\to\mathrm{A'B'}}|^2 = \int d^4x\, \frac{d^4q}{(2\pi)^4}\, A_{\mu\nu}(x,q)\, J_{\mathrm{B}}^{\mu\nu}(x,q)\,.$$

Here $J_{\mathrm{B}}^{\mu\nu}(x,q)$ is the Wigner transform of current B and $A_{\mu\nu}(x,q)$ is the Wigner transform of the photon field created by the current A. $A_{\mu\nu}(x,q)$ is written in terms of the Wigner transforms of the current A and the photon propagator:

$$A_{\mu\nu}(x,q) = \int d^4y\, D_{\mu\nu\mu'\nu'}(x-y,q)\, J_{\mathrm{A}}^{\mu'\nu'}(y,q)\,.$$

If we compare this S–matrix to the S–matrix of the one photon absorption process shown in figure 2,

$$|S_{\gamma\mathrm{B}\to\mathrm{B'}}|^2 = \int d^4x\, \frac{d^4q}{(2\pi)^4}\, \frac{\pi}{q_0} \sum_{\mathrm{pol}} \epsilon^{\mu}(\lambda)\, \epsilon^{*\nu}(\lambda)\, (2\pi)^4\, \delta^4(q-k)\, J_{\mathrm{B}}^{\mu\nu}(x,q)\,,$$

we can identify the Effective Photon Distribution. In the gradient approximation ($\partial/\partial x^{\mu} \ll q_{\mu}$), it is

$$\frac{dn(x,q)}{d^4x\, d^4q} = \frac{q_0}{4\pi} \sum_{\mathrm{pol}} \epsilon^{\mu}(\lambda)\, \epsilon^{*\nu}(\lambda)\, A_{\mu\nu}(x,q)\,.$$

This result is of limited usefulness; in at least one important case the gradient expansion is inapplicable. For the case of a massive point particle with trajectory $y_{\mu} = y_0 v_{\mu}$ and four–velocity $v_{\mu} = (1, \vec{\beta})$, where $\beta \approx c$ and $\gamma = 1/(1-\beta^2)$, we find the $A_{\mu\nu}(x,q)$:

$$A_{\mu\nu}(x,q) = \frac{32\pi^2\alpha\gamma\delta(q\cdot v)}{\sqrt{-q^2}} v_{\mu}v_{\nu}\mathcal{A}\Big(2|x\cdot q|, 2\sqrt{-q^2\gamma^2\left((x\cdot v)^2 - x^2v^2\right) - (x\cdot q)^2}\Big)\,.$$

$\mathcal{A}(a,b)$ is a strongly peaked function with the peak centered on $(a,b) = (0,0)$ and a radius of 2. One can imagine the resulting $A_{\mu\nu}(x,q)$ to be a "Lorentz contracted onion" centered on the point source. The inner layers of the "onion" correspond to higher energy energy photons. Each layer has radius $1/\gamma\sqrt{-q^2}$ in the $\vec{\beta}$ direction and radius $1/\sqrt{-q^2}$ in the transverse direction. Clearly taking derivatives of this $A_{\mu\nu}(x,q)$ gives answers proportional to q_{μ}, demonstrating the inapplicability of the gradient approximation. Nevertheless, applying the classical arguments of Jackson [4], we Wigner transform the $\vec{E}$–field of this point particle and find the Effective Photon Distribution shown in figure 3.

We can now ask how virtual partons interact such as in the two photon process in 4. This process contains the subprocess $\gamma \to e\bar{e}$:

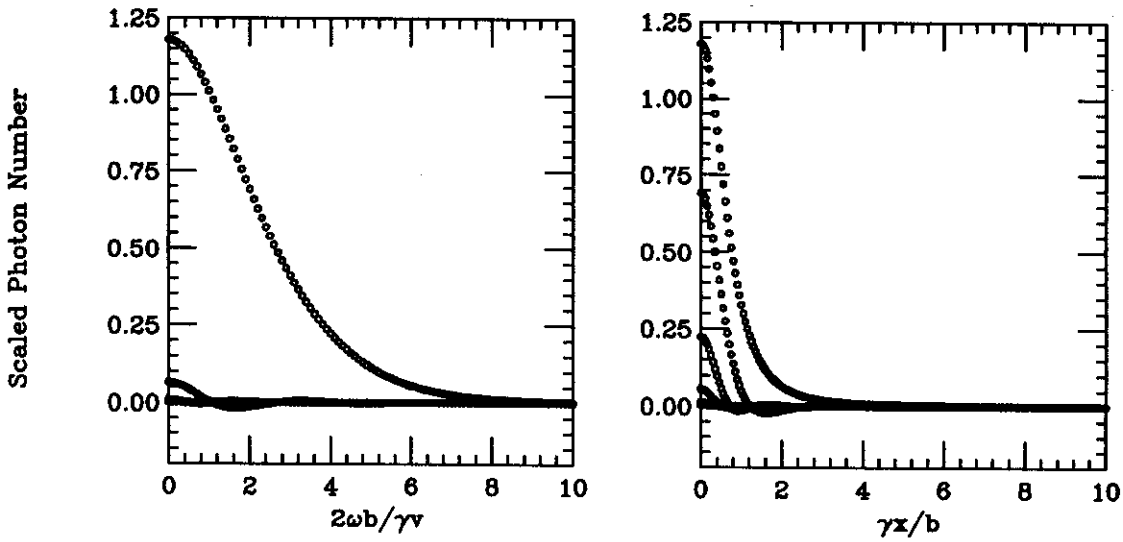

Figure 3: The Effective Photon Distribution integrated over $\vec{q}$. b is the impact parameter and x is the longitudinal coordinate. In the left figure, the largest curve is the distribution at $\gamma x/b = 0$ and subsequent curves are in steps of 2 in $\gamma x/b$. In the right figure, the largest curve is the distribution at $2\omega b/\gamma v = 0$ and subsequent curves are in steps of 2 in $2\omega b/\gamma v$.

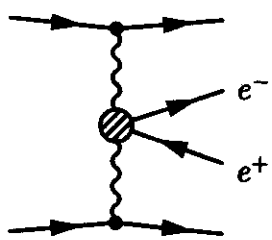

Figure 4: Lepton pair production

This process can only occur when the high energy portions of the point charges' Effective Photon Distributions (with $q_0 g e q m_e$) overlap. This region has a characteristic size of $\sim 1/\gamma\sqrt{-q^2}$ but its actual shape is determined by the geometry of the collision. The interaction itself takes place in a sphere with radius $\sim 1/m_e$. Were the exchanged electron massless, the radius would be determined by the electron's virtuality since the size of this interaction region is determined by the lifetime of this electron. In this analysis, we cannot tell whether the distribution of the $e\bar{e}$ pairs produced by the subprocess $\gamma \rightarrow e\bar{e}$ are Lorentz contracted without cutting the blob in figure 4.

From this analysis, we can extract several pieces of information about the phase–space PDF's and the structure of their partonic interactions. First, the gluons spawned by a bare quark (via $q \rightarrow qg$) should be spread out in a Lorentz contracted sphere with higher energy quarks distributed closer to the source quark. Second, an interaction such as $gg \rightarrow q\bar{q}$ takes place in the region where the higher energy portions of the gluons' PDF's overlap. The virtualities of the partons play an important role in both analyses: the width of a virtual parton distribution is determined by the parton's virtuality in its source's rest frame and the interaction region of colliding partons has a characteristic size determined by the exchanged parton's virtuality. We plan to analyse the process $\gamma \rightarrow e\bar{e}$ and determine what role the parton's virtuality plays in parton multiplication. Future extensions of this work might be to derive phase–space Gribov–Liputov–Altarelli–Parisi equations so that the phase–space PDF's might be derived from first principles or to construct a model hadron and determine its PDF's using the parton distributions derived here.

References

1. K. Geiger, Phys. Rev. D 46 (1992) 4965.
2. G. Altarelli and G. Parisi, Nucl. Phys. B126 (1977) 298.
3. C. Quigg. *Gauge Theories of the Strong, Weak and Electromagnetic Interactions.* Addison-Wesley, New York (1983).
4. J.D. Jackson. *Classical Electrodynamics.* John Wiley and Sons, New York (1975). pp. 668-669, 719-725.
5. E.A. Remler, Ann. Phys. 202 (1990) 351.
6. P. Carruthers and F. Zachariasen, Rev. Mod. Phys. 55 (1983) 245.

EXCESS DILEPTONS IN CERN SPS DATA

J. Murray, K. Haglin and W. Bauer

With the advent of higher energy nucleus-nucleus colliders, such as RHIC, the usual treatment of the individual nucleon-nucleon scattering is no longer appropriate. Relativistic heavy-ion collision simulations must incorporate QCD to describe the subnucleonic features. This incorporation of QCD is manifest in parton cascades which assume a quark-gluon plasma is formed during the collision and distribute partons instead of nucleons inside the colliding nuclei [1,2,3]. The partons are allowed to scatter and evolve in time until the energy density is low enough for hadronization to occur.

Whether or not a quark-gluon plasma can be experimentally detected depends largely on the characteristics of the collision if a plasma isn't formed. In order to describe the background to plasma formation as well as other high energy nuclear effects, simulations are needed that don't assume plasma formation, but still use QCD to describe nucleon scattering within the nucleus-nucleus collision. HIJING, developed by Wang and Gyulassy [4], is a model of the latter type which has been used to look at multiple minijet production and how it is affected by nuclear shadowing and jet quenching in pA and AA collisions.

The simulation we developed is similar to HIJING. The number of nucleon-nucleon collisions is determined geometrically and the individual nucleon-nucleon collisions are handled by PYTHIA and JETSET [5], typical high energy event-generators using QCD matrix elements and the Lund fragmentation scheme. In addition to looking at hadronic spectra as does HIJING, this model can also look at dilepton production. In order to accomplish this, several hadronic decay modes have been added to those already inside JETSET, such as $\eta' \to \gamma e^- e^+$, $\omega \to \pi^0 e^- e^+$, $\omega \to e^- e^+$, $\phi \to e^- e^+$. To model these decays, we need the differential decay width, $d\Gamma/dM^2$, where M^2 is the invariant mass of the dilepton pair and $|\mathcal{M}|^2$, the matrix element squared, to Monte Carlo the invariant mass and the final momenta of the dilepton pair.

The model can be used to study dilepton production at CERN SPS [6], for example. In Fig. 1 we compare with the low-mass spectrum from proton induced interactions. The data plotted is the invariant mass spectrum of dilepton pairs from hadronic decays.

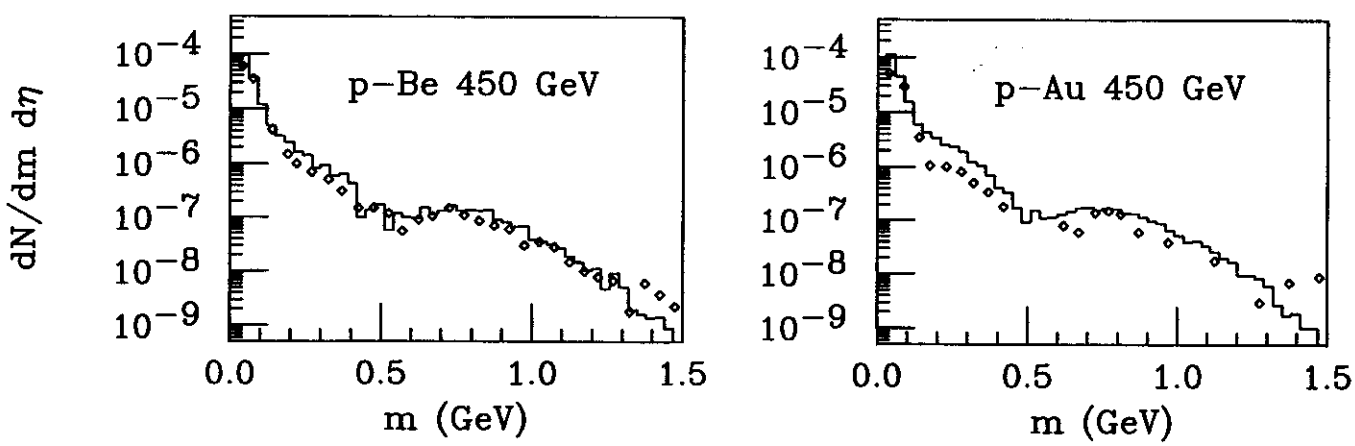

Figure 1: Simulation comparisons to data with kinematic cuts, $p_t > 50$ MeV/c, $\Theta_{ee} > 35$ mrad, $2.1 < \eta < 2.65$

In the pA system, dileptons from decaying hadrons (π^0, η, $\eta\prime$, ρ^0, ω, and ϕ) describe the experimental data. In the S-Au at E_{LAB} = 200 GeV system, there is an excess of dileptons with invariant mass between 200 MeV/c^2 and about 1 GeV. The hadronic dilepton decays no longer account for the observed dileptons. It was recently proposed that the excess might be due to secondary π ρ and π π scattering [7]. Dileptons from π π scattering come from $\pi\pi \rightarrow \rho^0 \rightarrow e^- e^+$. At the present we will only consider the resonance channel for π ρ scattering, $\pi\rho \rightarrow a_1 \rightarrow \pi e^- e^+$. Rescattering of final state π's and ρ's will be incorporated into the model to determine whether or not these scatterings can explain the excess of observed dileptons.

References

1. K. Geiger and B Müller, Nucl. Phys. A544 (1992), 467c.
2. K. Geiger and B. Müller, Nucl. Phys. B369(1992), 600.
3. G. Kortemeyer, J. Murray, S. Pratt, K. Haglin, and W. Bauer, NSCL Annual Report (1993), 63.
4. X. Wang and M Gyulassy, Phys. Rev. D44 (1991), 3501.
5. CERES Collaboration, Phys. Rev. Lett. 75 (1995), 1272.
6. T. Sjöstrand, Computer Physics Commun 82 (1994) 74.
7. K. Haglin, Phys. Rev. C53, June 1996.

DYNAMICAL EFFECTS IN THE FISSION OF HOT NUCLEI

M. Thoennessen

The influence of dissipation on the formation and decay of compound nuclei has been known for a long time. Initially only the dissipation from the saddle-to-scission motion in the fission process [1] and the hindrance of fusion in heavy-ion collisions [2] have been considered. The observation of an enhanced emission of pre-fission neutrons, protons, and γ-rays in the fission of hot nuclei opened up the opportunity to study the detailed influence of dissipation on the total fission process [3,4].

Fission as a decay mode of heavy compound nuclei was first described with the transition state model [5], where the fission decay width Γ_{trans} is given by:

$$\Gamma_{trans} = \frac{1}{2\pi\rho(E)} \int_0^{E-E_B} \rho^*(E - E_B - \epsilon)d\epsilon \tag{1}$$

where E_B is the fission barrier, E the excitation energy and ρ the compound nuclear level density. ρ^* is the "... density of all levels which arise from excitation of all degrees of freedom other than fission itself." [5]. With the explicit distinction between ρ and ρ^* equation 1 can be approximated by

$$\Gamma_{trans} = \frac{\hbar\omega_{eq}}{2\pi} exp(-E_B/T) \tag{2}$$

Kramers introduced fission as a dynamical process and calculated the fission decay width Γ_{Kra} as a function of dissipation [6] which can be written as:

$$\Gamma_{Kra} = \frac{\hbar\omega_{eq}}{2\pi}(\sqrt{1+\gamma^2} - \gamma) exp(-E_B/T) \tag{3}$$

with the temperature T and the nuclear friction coefficient γ. Kramers derived this equation in terms of the viscosity parameter η which is directly related to γ via: $\eta = 4\pi\omega_{sp}\gamma$ and the curvature of the saddle point is taken to be $\omega_{sp} = 1 \cdot 10^{21} s^{-1}$. Thus, the Kramers fission width corresponds to the transition state width, modified by the factor $\sqrt{1+\gamma^2} - \gamma$.

The incorporation of the dynamical model into a statistical model code like CASCADE involves several approximations which might play an important role in the results of the calculations. Statistical models do not depend on intrinsic quantities like the shape of the barrier and the fission decay width of the statistical model differs from the transition state model decay width as approximated in Equation 2.

In the statistical model the two level densities of equation 1 are set equal $\rho = \rho^*$ and the fission decay width used in statistical model codes can be expressed as:

$$\Gamma_{stat} = \frac{T}{2\pi} exp(-E_B/T) \tag{4}$$

Thus, the transition state value and the statistical model value are not identical and are related via:

$$\Gamma_{trans} = \frac{\hbar\omega_{eq}}{T}\Gamma_{stat} \tag{5}$$

This difference has actually been known for a long time [7] but it is usually not taken into account and the approximation $\hbar\omega_{eq} = T$ is typically made in the analyses.

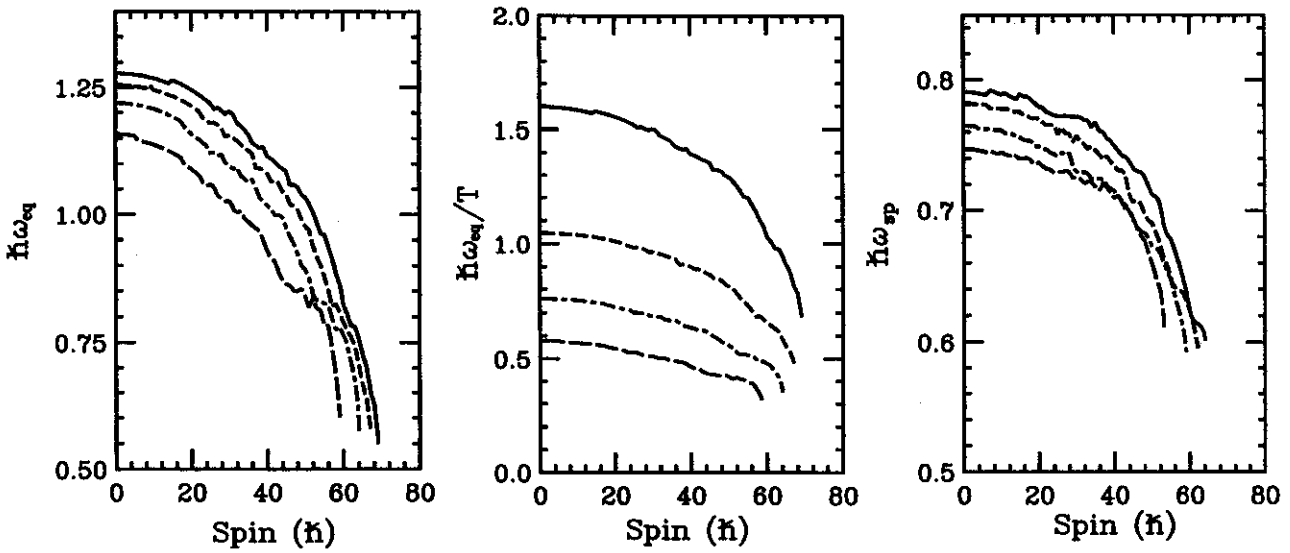

Figure 1: Curvature of the potential (left) and the ratio of the curvature over the temperature (middle) as a function of spin for ^{200}Pb at temperatures of 0.8 MeV (solid), 1.2 MeV (short-dashed), 1.6 MeV (dot-dashed) and 2.0 MeV (long-dashed). Right: Dissipation coefficient γ (top) and the resulting reduction of the fission width ($\Gamma_{Kra}/\Gamma_{trans}$) (bottom) as a function of excitation energy for the reaction ^{19}F + ^{200}Pb at 120 MeV.

It is not obvious that this approximation should be valid, because the decay of the compound nucleus covers a wide range of temperatures and the curvature at the equilibrium deformation (assault frequency) certainly changes with increasing angular momentum until the barrier vanishes. The left side of Figure 1 shows the assault frequency as a function of compound nuclear spin for different temperatures for ^{200}Pb. The calculations were performed based on the finite range liquid drop model and the parameterization of Lestone [8,9]. The average value of $\hbar\omega_{eq}$ is around 1 MeV. However, it varies considerably especially towards larger spins close to the vanishing of the barrier. The middle panel of Figure 1 shows the ratio of the curvature over the temperature $\hbar\omega_{eq}/T$. The approximation of the statistical model assumes this value to be constant equal to unity. As can be seen, the ratio is certainly not constant and varies in the present range from ~ 0.5 to ~ 1.6, which could certainly have a significant influence on the calculation of pre-fission particle emission probabilities and particle multiplicities.

In order to investigate the potential effects of this approximation, we incorporated the temperature and spin dependence of the equilibrium curvature shown in Figure 1 in the standard statistical model code CASCADE. The calculation was based on the Bohr-Wheeler description and did not include the dynamical effects of Kramers. The results for the reaction ^{19}F + ^{200}Pb at E_{Beam} = 120 MeV show a slightly larger pre-fission neutron multiplicity and a significantly reduced evaporation residue cross section inconsistent with the experimental results [10]. Thus, this modification cannot account for the measured excess pre-fission neutron multiplicity and a dynamical description of the fission process is necessary to describe the data.

Another approximation that was applied in equation 3 was the value of the curvature of the barrier which was taken to be $\omega_{sp} = 1 \cdot 10^{21} s^{-1}$. This influences directly the conversion of the friction parameter γ to the reduced dissipation coefficient β which are related via the equation $\gamma = \beta/2\omega_{sp}$. The assumption of a constant $\omega_{sp} = 1 \cdot 10^{21} s^{-1}$ yields $\gamma = \beta/2 \cdot 10^{-21} s$, which is typically used [3]. However, right panel of Figure 1 shows the curvature as a function of the compound nucleus spin for different

temperatures for ^{200}Pb . Again, these calculations were performed with the finite range liquid drop model using the parameterization of Lestone [8,9]. Although the average value is $\hbar\omega_{sp} \sim 0.75MeV$ corresponding to $\omega_{sp} \sim 1 \cdot 10^{21} s^{-1}$ there is a rather large spread which is strongly temperature as well as spin dependent. Thus no direct conversion between γ and β is possible, and the comparison of results with analyses based on the two different dissipation constants should be treated with caution.

References

1. J. R. Nix and A. J. Sierk, *Proc. 6th Adriatic Int. Conf. on Nucl. Phys.: Frontiers in Heavy-Ion Physics*, p.333 (1990).
2. W. J. Swiatecki, Phys. Scr. 24, 113 (1981).
3. D. Hilscher and H. Rossner, Ann. Phys. Fr. 17, 471 (1992).
4. P. Paul and M. Thoennessen, Ann. Rev. Nucl . Part. Sci. 44, 65 (1994).
5. N. Bohr and J. A. Wheeler, Phys. Rev. 56, 426 (1939).
6. H. A. Kramers, Physica VII, 284 (1940).
7. V. M. Strutinski, Phys. Lett. B47, 121 (1973).
8. J. P. Lestone, Phys. Rev. C 51, 580 (1995).
9. R. C. Lemmon, private communication.
10. M. Thoennessen, *Proc. of the Groningen Conference on Giant Resonances*, Nucl. Phys. A, in print (1996).

INFLUENCE OF FORMATION TIMES ON EVAPORATION RESIDUES

M. Thoennessen

Evidence for reaction dynamical effects in the formation and decay of compound nuclei is still quite controversial [1,2]. In measurements of the γ-ray decay of the giant dipole resonance (GDR) differences in the reactions ^{64}Ni + ^{100}Mo and ^{16}O + ^{148}Sm forming the same compound nucleus ^{164}Yb were observed [3]. While the γ-ray spectrum following the latter reaction could be described, the former showed significant deviations from the statistical model calculations.

These differences could be explained within the dissipative dynamical model [4,5] which predicts long formation times for certain almost symmetric heavy-ion fusion reactions. The differences in the GDR spectra arise from these formation times during which particle and γ-ray can occur which changes the population of the initial compound nuclei. This difference in the initial population could also result in differences in the final spin distribution of the evaporation residues which might be important for the reaction-dependent feeding of superdeformed bands [6] which have recently been reported [7,8]. Again, these observations are still controversial [9-12].

In order to search for possible effects of the formation time on the population of superdeformed bands calculations for the decay of the compound nucleus ^{164}Yb formed with the reaction ^{64}Ni + ^{100}Mo were performed. From the semiclassical code HICOL [13] which is based on Swiatecki's model it is possible to extract in addition to the total compound nucleus formation time, the time evolution of the internal excitation energy as a function of time. If the formation times become comparable to the neutron evaporation times the contribution of evaporation during the formation stage can become important for the subsequent decay of the compound nucleus.

For the reaction ^{64}Ni + ^{100}Mo, HICOL predicted formation times of $\sim 10^{-20}s$ which are comparable to neutron evaporation times ($1.6 \cdot 10^{-20}s$) for ^{164}Yb at 49 MeV excitation energy, whereas for more asymmetrically formed and/or lighter systems the formation times are much shorter than the evaporation times. In a first approach to incorporate the evaporation during the formation times into the statistical model, the formation stage was treated not time dependent, but average values for the excitation energy and shape were used [1,3].

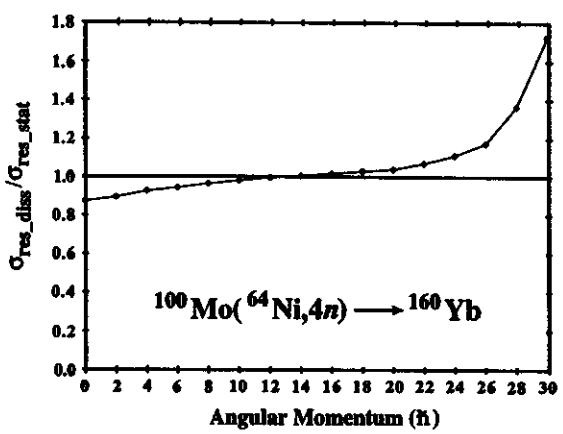

Figure 1: Ratio of the spin dependent 4n evaporation residue cross section of the standard statistical model over the model including evaporation during formation.

As an example for possible effects of the formation on the population of superdeformed bands we studied the population of the Yrast line of the 4n evaporation channel populating ^{160}Yb with the standard statistical model and with the modified model which included decay during the formation stage. The overall particle multiplicity for both cases was exactly the same and thus the cross section for populating ^{160}Yb was identical. However, the population distribution of the Yrast line was indeed shifted towards larger spin for the latter calculation.

Figure 1 shows the ratio of the cross section for the dissipative calculation which included the formation time (σ_{res_diss}) and the standard statistical model calculation (σ_{res_stat}) as a function of spin. It is apparent that the incorporation of the formation times reduces the population at low spins and enhances the population at larger spins, which would thus favor the population of superdeformed bands. Although this effect is fairly small because it only effects the tails of the distributions, it might become important for the population of superdeformed bands.

In conclusion, the calculations show that the formation time can influence the evaporation population of residues. However, these initial calculations have to be taken with care and have to be verified for each specific case. It is certainly possible that in other cases the formation time could enhance the lower spins or would not effect the distribution at all.

References

1. M. Thoennessen *et al.*, Phys. Rev. C 51, 3148 (1995).
2. F. Heller, Ph.D. Thesis, Heidelberg, MPI-H-U13 (1995).
3. M. Thoennessen *et al.*, Phys. Rev. Lett. 70, 4055 (1993).
4. J. Blocki *et al.*, Ann. Phys. (N.Y.) 105, (1977).
5. W. J. Swiatecki, Physica Scripta 24, 113 (1981).
6. M. Thoennessen and J. R. Beene, Phys. Rev. C 45, 873 (1992).
7. G. Smith *et al.*, Phys. Rev. Lett. 68, 158 (1992).
8. S. Flibotte *et al.*, Phys. Rev. C 45, R889 (1992).
9. S. M. Mullins *et al.*, Phys. Lett. B312, 272 (1993).
10. S. M. Mullins *et al.*, Phys. Rev. C 52, 99 (1995).
11. F. Soramel *et al.*, Phys. Lett. B350, 173 (1995).
12. G. Viesti *et al.*, Proc. of the "First Latinamerican Workshop on: On and Off Beam Gamma Spectroscopy for the Study of Heavy Ion Reaction and Pre-equilibrium Processes", September 4-8, 1995, Caracas, Venezuela, to be published in Heavy Ion Physics (1996).
13. H. Feldmeier, Rep. Prog. Phys. 50, 915 (1987).